GSA Data Repository 2016135

Late Cretaceous unroofing of the White Mountains, New Hampshire, USA: An episode of passive margin rejuvenation?

W.H. Amidon et al.

Sampling and Methods

The core was drilled in the broad valley of the Saco river at the point where it turns east, exiting the confines of the modern White Mountain topography (Fig. 1). Sections of drill core were obtained from -122, -402, and -695 m asl, supplemented by a surface samples from the drilling site (204 m asl), and from a nearby ridgeline (515 m asl) for a total vertical relief of ~1300 m (Fig. 2). The 1.75" diameter core penetrated four major granitic units. The upper ~365 m penetrates the green phase of the Conway granite, followed by the red phase to a depth of ~730 m, the Albany Syenite for the next 120 m, and a hornblende-biotite granite for the final 60 m (Hoag and Stewart, 1977). The temperature at the bottom of the drill hole was measured at 33°C giving a thermal gradient of 30.3 °C/km relative to the mean surface temperature of 5.4°C. This surprisingly high gradient is consistent with anomalous radiogenic heat production in these granitic phases, which is the reason the core was drilled.

Apatite and zircon were separated following standard procedures and AHe analyses were performed at the Berkeley Geochronology Center (BGC) and at the TRAIL lab at UC Boulder. Apatite size and yield varied widely, which is why we do not have AFT data for sample V16 and V14. Apatite was so sparse in sample V14 that only two suitable grains were found for AHe analysis.

Here we describe the methods used by the TRAIL laboratory, which are similar to those used by the BGC lab (e.g. Tremblay et al., 2015). Individual mineral grains are handpicked using a SMZ 1000 binocular microscope equipped with a calibrated digital camera and capable of both reflected and transmitted, polarized light. The grains are screened for quality, including crystal size, shape, and the presence of inclusions. After characterization, grains are placed into small Nb tubes that are then

crimped on both ends. This Nb packet is then loaded into an ASI Alphachron He extraction and measurement line. The packet is placed in the UHV extraction line (~3 X 10^{-8} torr) and heated with a diode laser to ~800°C for 5 minutes to extract the radiogenic ^{4}He. The degassed ^{4}He is then spiked with approximately 13 ncc of pure ^{3}He, cleaned via interaction with two SAES getters, and analyzed on a Balzers PrismaPlus QME 220 quadrupole mass spectrometer. Degassed grains are then removed from the line, and taken to a Class 10 clean lab for dissolution. Apatite grains, still enclosed in the Nb tubes, are placed in 1.5 mL Cetac vials, spiked with a calibrated ^{235}U – ^{230}Th – ^{145}Nd mixture in HNO_3, capped, and baked in a lab oven at 80°C for 2 hours. Once the minerals are dissolved they are diluted with 1 mL of doubly-deionized water, and taken to the ICP-MS lab for analysis. Sample solutions, along with standards and blanks, are analyzed for U, Th, Nd, and Sm content using a Thermo Element 2 magnetic sector mass spectrometer. Once the U, Th, and Sm contents have been measured, He dates and all associated data are calculated using data reduction methods specific to the lab. Shards of Durango apatite used as an external standard gave results of 31.8 ± 1.3 (n=12).

Apatite Fission Track (AFT) analyses were performed at SUNY Plattsburgh using the external detector method for age determinations. Small aliquots of apatite were mounted in epoxy on glass slides and polished to expose internal grain surfaces. Spontaneous fission tracks were revealed by etching for 20 s in 5 M HNO3 at 21°C. The samples were irradiated at the Oregon State University TRIGA reactor using a nominal flux of 8x10^{15} n/cm^2. CN1 dosimeter glasses were used to monitor the neutron flux at the top and bottom of the irradiation tube. Fission-track ages were calculated using a weighted mean zeta (ζ) calibration factor of 98.4 based on Fish Canyon Tuff, Durango, and Mount Dromedary apatite standards (Hurford and Green, 1983; Miller et al., 1985). Age determinations and length measurements were made dry on an Olympus BMAX 60 microscope at 1600x. This microscope is equipped with a drawing tube for length measurements, which were digitized on a drawing slate. The AFT ages were determined as central ages using the HeFTy program, version 1.8.3 (Ketcham, 2005).

U-Pb analyses on zircon and U/Th zonation profiles were performed by LA-ICPMS at RPI following published methods described in Amidon et al., 2015 and Farley et al., 2011, respectively. All LA-ICPMS analyses were done using a Photon Machines Analyte 193 excimer laser coupled to a Bruker 820 quadrupole ICPMS with initial data reduction in Iolite v. 2.5 (Paton et al., 2011). For zircon analyses, a spot size of 30 μm was used with a repetition rate of 4 Hz. Isotopic fractionation and drift were standardized using the FC-Z5 zircon standard (Paces and Miller, 1993) and validated using R33 as a secondary standard (Black et al., 2004). The mean resultant age of the R33 standard was 418 ± 3.2 with a MSWD of 1.2. U-Pb ages were calculated using the Isoplot software (Ludwig, 2008). Quoted ages are corrected for common Pb by assuming an initial $^{207}Pb/^{206}Pb$ ratio of 0.847 and using the 'Age207cor', function in Isoplot. No correction is applied for initial disequilibrium in the U decay series.

Apatite zonation measurements were made on approximately 20 grains per sample, by taking 3-5 transects perpendicular to the c-axis. Only 2 grains were analyzed for sample V14 due to a severe paucity of apatite in the sample. We used a spot size of 15 μm, a repetition rate of 6 Hz, and a velocity of 1 μm/sec. In addition to ^{238}U and ^{232}Th, ^{140}Ce was also measured to determine when the laser was analyzing apatite and ^{44}Ca was measured to normalize sensitivity changes (e.g. Longerich et al., 1996). A major issue with LA-ICPMS zonation measurements is defining when the signal can be considered representative of the grain versus when it is simply measuring residual material in the ablation chamber and flow line. In this case, we defined the grain boundary as the time when the ^{140}Ce signal was above 50% of the lowest ^{140}Ce signal observed in the interior of the grain. Raw time series data was reduced in Matlab following the methodology of Farley et al., 2011, using Durango apatite as a primary standard and Madagascar apatite as a secondary standard (Thomson et al., 2012). Estimated U and Th concentrations of the Madagascar standard were factors of 1.08 ± 0.04 and 1.19 ± 0.12 higher than the reported values respectively, although relative concentrations within a given transect should be accurate to within a few percent.

Apatite zonation measurements show that zonation varies widely by sample, and that grains can be generally categorized as unzoned, rim enriched, core enriched, or rim and core enriched (Fig. DR1). After categorizing zonation in each grain, average normalized zonation profiles were computed for each category of each sample. Simple rim enrichment was the most common type of zonation, appearing in 80%, 90%, 70%, and 50% of grains from V13, V15, V16, and V17 respectively. The average core-rim U/Th enrichment factors were large; 8, 9, 30, and 5 for samples V13, V15, V16, and V17 respectively. Weak or unzoned grains (<2x core-rim enrichment) were the next most common, occurring as in 0%, 10%, 15%, and 15% of grains from V13, V15, V16, and V17 respectively. Core-enriched grains were only observed in V16 (15%) and V17 (10%), whereas core and rim enriched were only observed in 13 (20%) and 17 (25%).

Cl and F concentrations in apatite were determined using a CAMECA SX-100 electron microprobe at RPI. We analyzed X-ray lines of major elements in apatite at 15KeV, 20nA, with a 10 μm spot size. The analytical routine included Ca Kα (on PET), P Kα (on TAP), F Kα (on LPC0), Cl Kα (on LPET), and Ce Lα (on LLIF). Ca and P were calibrated against apatite (Durango, Smithsonian collection), F against topaz (unknown locality, RPI collection), Cl using sodalite (Bancroft CAN, Harvard collection), and Ce using synthetic Ce-phosphate (RPI). All elements were analyzed for 30 seconds peak time, and 30 seconds background, except fluorine. Fluorine was measured for 15 seconds, subdivided into five 3-second periods for inspection of time-dependent intensity changes. Matrix corrections followed Pouchou and Pichior, (1990) with oxygen assigned stoichiometrically and adjusted for the measured halogen content (Pouchou and Pichoir, 1990).

Modeling

Much of the dispersion in AHe ages likely arises from differences in grain size, effective uranium (eU), and zonation patterns (Flowers et al., 2009; McKeon et al., 2014). Modeling a family of reasonable thermal histories is particularly challenging because zonation of specific grains used for AHe is unknown and varies widely for some samples. As a first step, we seek to understand the amount of dispersion that unknown zonation could induce on the observed ages. To do this, we implemented two forward models in HeFTY (Fig. 3) (Ketcham, 2005). A "linear"reference model assumed a long-term cooling rate of 1.5 °C/Ma, extrapolated backwards from the modern day temperature until intersecting a reasonable post-igneous cooling rate. A second "fitted" model was iteratively fitted to the combined AHe and AFT dataset, while honoring four criteria: 1) radiation damage kinetics following Flowers et al., 2009, 2) an initial temperature of 200 °C at 190 Ma for all samples to honor their common igneous cooling constraint, 3) a geothermal gradient held equal to modern during periods of slow cooling, 4) non-igneous cooling rates not to exceed ~13 °C/Ma (an erosion rate of ~ 0.5 mm/yr). This last constraint was included as an a priori geologic constraint to improve the efficiency of the modeling. It is based on the assumption that a rejuvenated passive margin terrane should not achieve cooling rates approaching those of the most active orogenic belts in the world. Although model results approached this rate (9-12 °C/Ma), they did not reach it, demonstrating that the assumption does not influence the model result. We recognize that thermal gradients change over time, but do not view our data as sufficiently precise to model such changes, and transient adjustments are unlikely to affect our first order conclusions.

Both forward models were run for each of the relevant zonation cases described above to gauge the effect of unknown zonation on inducing age dispersion. Model inputs were computed for each individual grain, by renormalizing the averaged zoning profile to match the bulk measured U and Th in that grain. Model results thus simulate what the observed age of that grain would be if its unknown zoning profile matched one of the zoning scenarios measured by LA-ICPMS on other grains from the same sample. Figure DR2 shows that the uncertainty induced by unknown zonation is much larger for

small high eU grains. Likewise, dispersion is magnified in the slowly cooled reference case relative to the fitted case in which all samples are rapidly cooled. Model results also show that dispersion can be mostly attributed to incorrect Ft corrections as opposed to differences in diffusion kinetics between grains.

Despite the effects of zonation, the best-fit t-T path is rather tightly constrained and shows that the combined AFT and AHe data require a period of accelerated cooling between ~ 85-65 Ma. The data require a period of rapid cooling for two reasons: 1) to achieve agreement between AFT and AHe ages from the same sample, and 2) to match relatively consistent AHe ages observed within certain samples whose apatite grains show a wide spread in eU contents and/or grain size (e.g. samples V13, V14, and V16). Accelerated Plio-Pleistocene cooling was not a model requirement, but produced slightly improved fits for samples V11 and 16, so was honored for all samples.

Although unknown zonation limits the utility of our data for inverse modeling, we used the software program QTQt to gain a sense of the range of permissible thermal histories, particularly in the intervals outside of rapid cooling (Gallagher, 2012). Both AFT and AHe ages were included in the model whose only prior constraint was a broad temperature constraint of 100 ± 50 °C at 100 Ma. For the sake of simplicity and model efficiency, grains were assumed to be unzoned. 10000 iterations of burn-in followed by 5000 model iterations, yielded likelihood and posterior chains with flat trajectories and rapid variation, suggesting the model had converged on a relatively narrow family of solutions. The expected model shows rapid cooling from ~90-60 Ma, and provides good agreement between observed and modeled ages (Figs. 3, DR3, and DR4).

We note one shortcoming of our model results, which is that the forward and inverse models consistently underestimate the AHe ages of sample V13, implying that the observed ages are anomalously old relative to other AFT and AHe ages in the dataset (Fig. DR2). This issue is clear in the

forward model result, which shows the best-fit cooling history for sample V13 is closer to V14 then V15, when it should be roughly equidistant if our proposed cooling history is correct (Fig. 3).

Captions for supplementary figures DR1-DR5

FigureDR: Typical zonation spectra obtained for Redstone apatites. Samples are grouped by sample within the four major zonation types that were observed. If a specific sample is not shown within a zonation category that type of zonation was not observed in the ~20 grains analyzed for that sample.

Figure DR2: Results of the "linear" (left) and "fitted" (right) models showing model predictions for each specific grain in the sample or for the central AFT age. Filled circles represent model predictions (including different assumed zoning cases), open circles represent observed data. We were forced to assume zonation because zonation was not measured directly on the grains that were used for bulk AHe analyses. Because measured AHe ages are Ft corrected assuming no zoning, the modeled AHe ages are all reported using Ft corrections for an unzoned grain even when the underlying model data were generated by assuming a zoned grain.

Figure DR3: Inverse model results from QTQt showing the range of accepted model fits for the three samples with both AFT and AHe data (V13, V15, and V17). Thin black line shows the 95% confidence interval and thick black line shows the best-fit expected model (a weighted mean of all accepted fits). The thick olive line shows the best-fit posterior model (the single-best fitting history).

Figure DR4: Best-fit ages from the expected model produced by QTQt assuming rim-enriched grains. Filled circles represent model predictions and open circles represent observed data. We were forced to

assume zonation because zonation was not measured directly on the grains that were used for bulk AHe analyses. Because measured AHe ages are Ft corrected assuming no zoning, the modeled AHe ages are all reported using Ft corrections for an unzoned grain even when the underlying model data were generated by assuming a zoned grain.

Figure DR5: Age-elevation plot of surface AFT ages within the grey box in figure 1. The inverse age-elevation relationship suggests focused denudation of the White Mountains relative to the Maine Coastal Plain during the same time interval. The one exception to this relationship is samples above ~800 m elevation, which are entirely from the Mt. Washington transect and show a positive age-elevation relationship. These ages were likely acquired during an earlier period of exhumation (>110 Ma) before differential exhumation began between the White Mountains and its surroundings.

Supplementary References Cited

Black, L. P., Kamo, S. L., Allen, C. M., Davis, D. W., Aleinikoff, J. N., Valley, J. W., Mundil, R., Campbell, I. H., Korsch, R. J., Williams, I. S., and Foudoulis, C., 2004, Improved 206Pb/238U microprobe geochronology by the monitoring of a trace-element-related matrix effect; SHRIMP, ID-TIMS, ELA-ICP-MS and oxygen isotope documentation for a series of zircon standards: Chemical Geology, v. 205, no. 1-2, p. 115-140.

Flowers, R. M., Ketcham, R. A., Shuster, D. L., and Farley, K. A., 2009, Apatite (U-Th)/He thermochronometry using a radiation damage accumulation and annealing model: Geochimica Et Cosmochimica Acta, v. 73, no. 8, p. 2347-2365.

Gallagher, K., 2012, Transdimensional inverse thermal history modeling for quantitative thermochronology: Journal of Geophysical Research, v. 117, no. B02408, p. doi:10.1029/2011JB008825.

Hoag, R. B., Jr., and Stewart, G. W., 1977, Preliminary petrographic and geophysical interpretations of the exploratory geothermal drill hole and core, Redstone, New Hampshire.

Hurford, A. J., and Green, P. F., 1983, The zeta age calibration of fission track dating: Chemical Geology, v. 1, p. 285-317.

Ketcham, R. A., 2005, Forward and inverse modeling of low-temperature thermochronometry data: Reviews in Mineralogy and Geochemistry, v. 58, no. 1, p. 275-314.

Longerich, H. P., Jackson, S. E., and Günther, D., 1996, Laser ablation inductively coupled plasma mass spectrometric transient signal data acquisition and analyte concentration calculation: Journal of Analytical Atomic Spectrometry, v. 11, no. 9, p. 899-904.

McKeon, R. E., Zeitler, P. K., Pazzaglia, F. J., Idleman, B. D., and Enkelmann, E., 2014, Decay of an old orogen: Inferences about Appalachian landscape evolution from low-temperature thermochronology: Bulletin of the Geological Society of America, v. 126, no. 1-2, p. 31-46.

Miller, D. S., Green, P. F., Hurford, A. J., and Naeser, C. W., 1985, Results of interlaboratory comparison of fission-track age standards: Nuclear Tracks and Radiation Measurements, v. 10, p. 381-391.

Paces, J. B., and Miller, J. D., 1993, Precise U-Pb ages of Duluth Complex and related mafic intrusions, northeastern Minnesota: geochronological insights to physical, petrogenetic, paleomagnetic, and tectonomagmatic processes associated with the 1.1 Ga Midcontinent Rift system: Journal of Geophysical Research, v. 98, no. B8, p. 13,997-"914,013".

Paton, C., Hellstrom, J., Paul, B., Woodhead, J., and Hergt, J., 2011, Iolite: Freeware for the visualisation and processing of mass spectrometric data: Journal of Analytical Atomic Spectrometry, v. 26, no. 12, p. 2508-2518.

Pouchou, J. L., and Pichoir, F., 1990, Surface film X-ray microanalysis: Scanning, v. 12, no. 4, p. 212-224.

Thomson, S. N., Gehrels, G. E., Ruiz, J., and Buchwaldt, R., 2012, Routine low-damage apatite U-Pb dating using laser ablation-multicollector- ICPMS: Geochemistry, Geophysics, Geosystems, v. 13, no. 1.

Examples of U-Th Zonation Transects

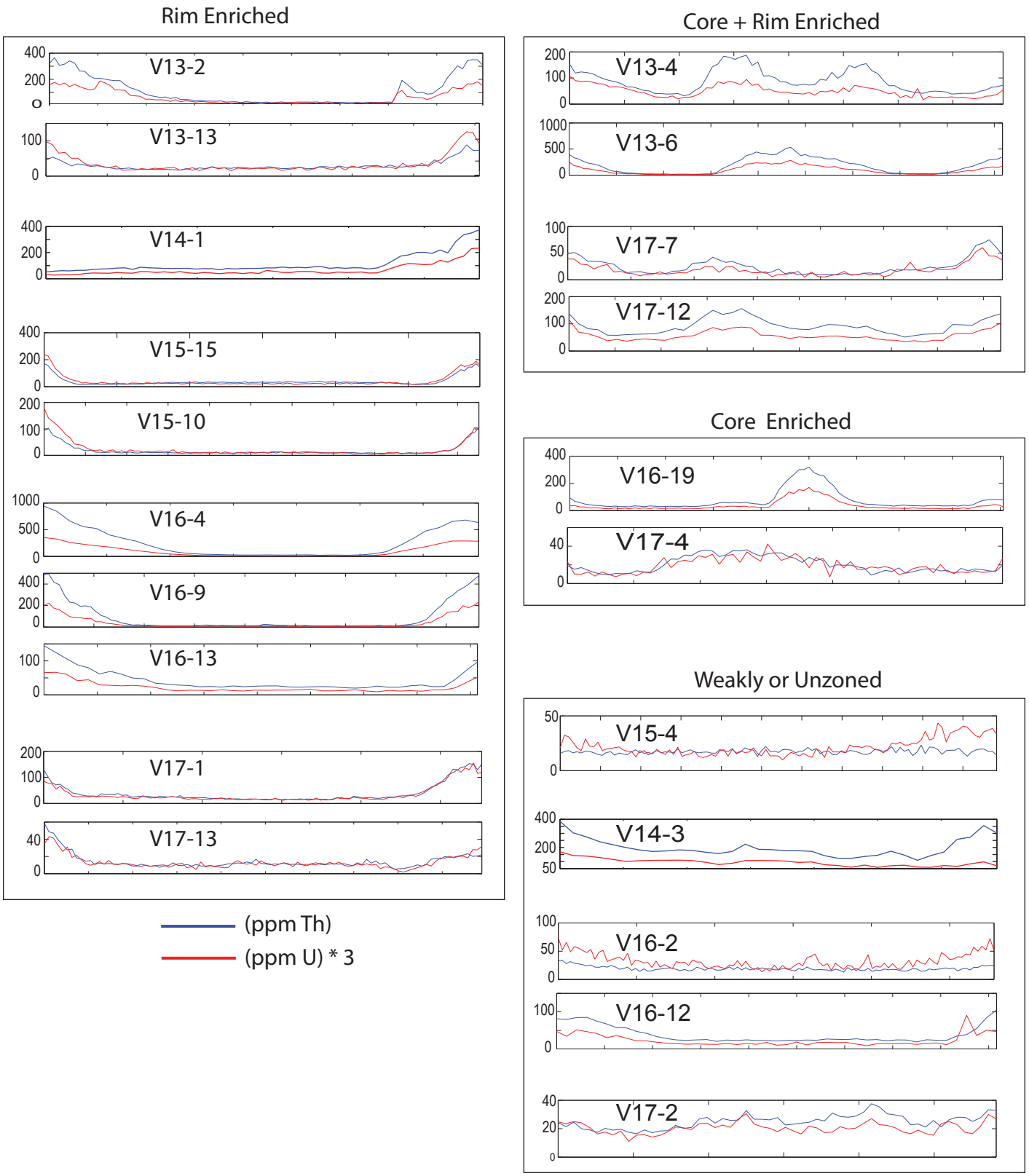

Amidon et al.
Supplementary Figure DR1

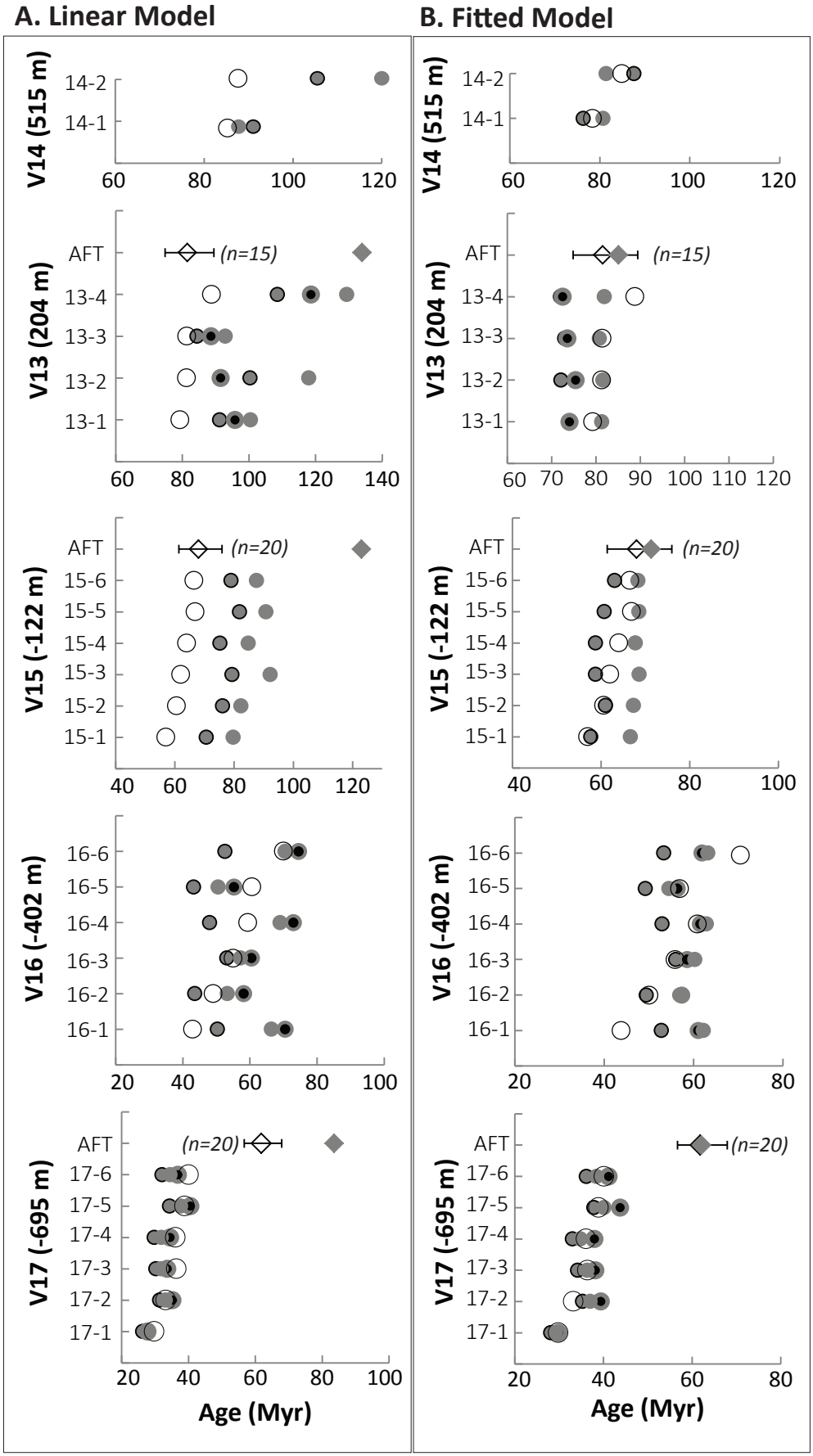

Modeled Ages (Ft assumes unzoned):

Enriched Rim Enriched Rim + Core Unzoned AFT Age

Computed Ages (Ft assumes unzoned):

(U/Th-He) Age Mean AFT Age

Amidon et al. Supplementary Figure DR2

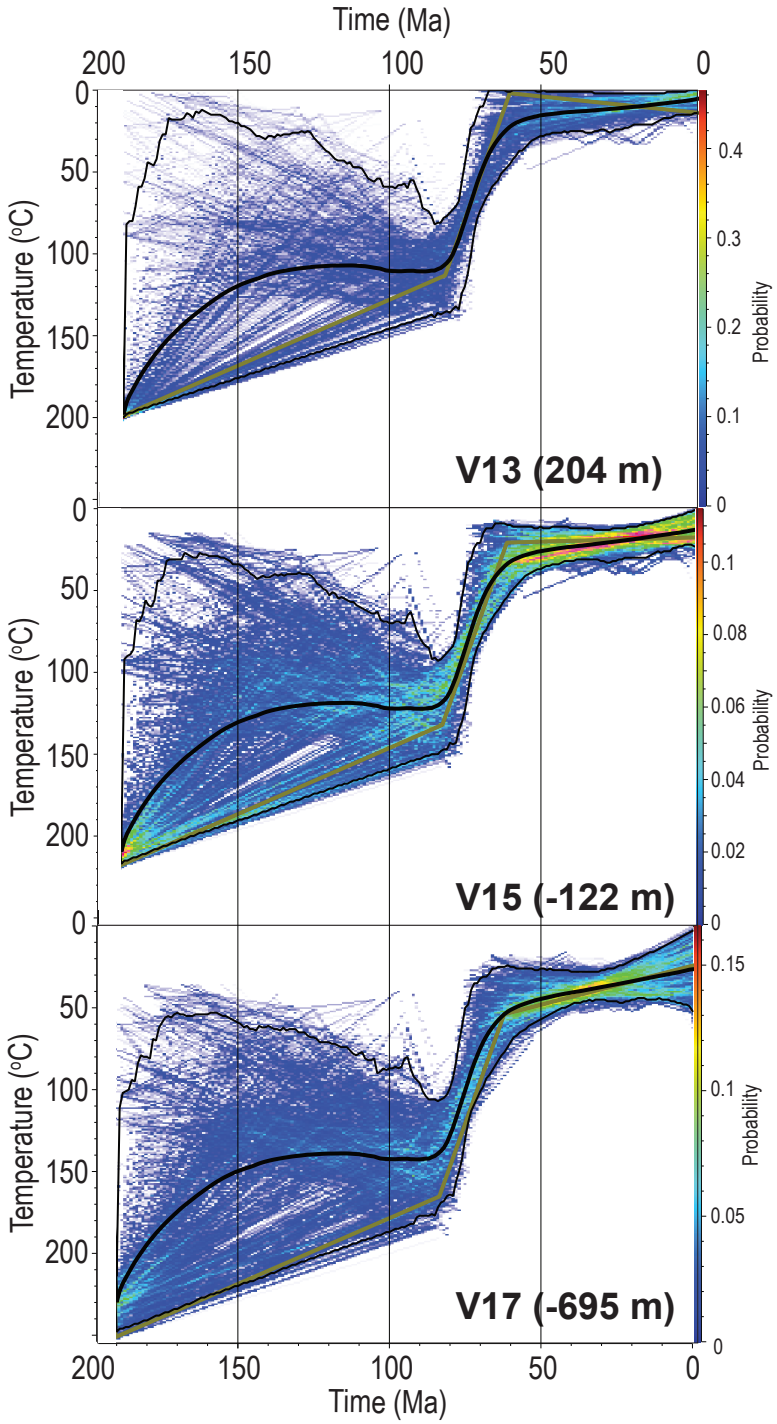

Amidon et al.
Supplementary Figure DR3

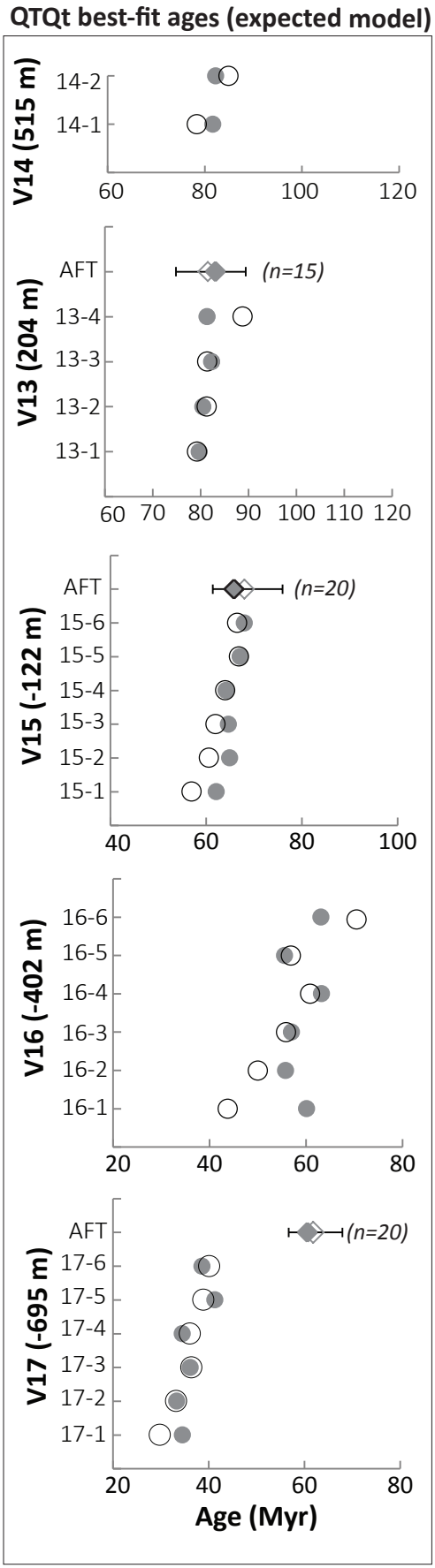

Modeled Ages (Ft assumes unzoned):

● Unzoned ◆ AFT Age

Computed Ages (Ft assumes unzoned):

○ (U/Th-He) Age ◇ Central AFT Age

Amidon et al.
Supplementary
Figure DR4

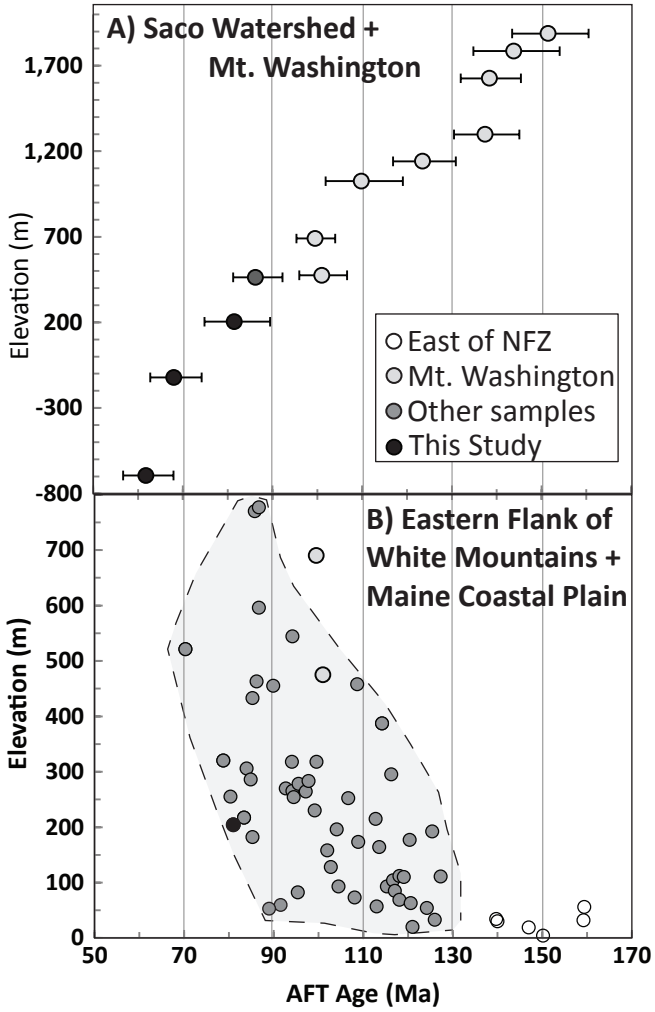

Amidon et al.
Supplementary Figure DR5

Supplementary Table DR1: Apatite U-Th/He Results

Sample	Elev. (m)	Length (um)	Width (um)	Radius (um)	FT	^{4}He (nmol/g)	1σ (nmol/g)	U (ppm)	1σ (ppm)	Th (ppm)	1σ (ppm)	Sm (ppm)	1σ (ppm)	Eu (ppm)	Raw Age (Ma)	1σ (Ma)	Cor. Age (Ma)	1σ (Ma)
v14-1	514	121	84	55	0.71	3.53	0.00	3.1	0.2	30.6	0.9	551.5	17.1	10	60.6	1.7	85.9	6.6
v14-2	514	130	80	46	0.66	26.85	0.05	6.0	0.9	26.0	2.9	400.0	27.5	12	59.4	0.8	90.3	8.5
V13-1	204	327	202	116	0.73	8.75	0.02	11.3	0.3	44.5	0.8	570.6	34.2	22	71.3	1.2	97.9	3.4
V13-2	204	318	186	107	0.70	28.96	0.04	30.9	1.3	182.8	5.3	695.3	13.1	74	71.5	1.7	101.6	7.5
V13-3	204	283	154	100	0.68	6.01	0.01	7.3	0.3	31.3	0.8	480.7	22.1	15	72.3	1.6	105.5	5.1
V13-4	204	367	178	104	0.70	65.66	0.05	64.9	0.8	386.3	2.8	1077.9	28.0	156	76.6	1.7	110.1	3.2
V13-5	204	284	168	96	0.67	7.68	0.01	6.0	0.4	39.1	0.9	300.6	13.5	15	91.4	2.4	136.4	9.6
V13-6	204	275	160	92	0.66	7.98	0.02	7.6	0.4	28.7	0.6	360.6	22.2	14	100.2	3.1	151.6	10.9
V15-1	-122	318	179	93	0.84	3.70	0.01	10.1	0.2	15.2	0.2	273.4	9.3	14	48.5	0.7	58.1	1.5
V15-2	-122	340	219	125	0.87	2.88	0.00	6.1	0.1	15.0	0.5	49.9	1.3	10	54.8	0.8	62.7	4.4
V15-3	-122	396	207	109	0.86	8.98	0.02	20.5	0.1	40.0	0.3	264.0	10.6	30	54.4	0.9	63.4	1.4
V15-4	-122	421	181	108	0.85	5.32	0.01	10.8	0.1	27.2	0.3	297.1	11.9	17	55.7	0.8	65.2	1.6
V15-5	-122	353	247	123	0.87	7.18	0.01	14.4	0.3	32.2	0.4	63.4	0.9	22	59.9	0.8	68.6	4.9
V15-6	-122	189	216	140	0.89	2.49	0.00	4.7	0.1	11.4	0.3	60.8	1.6	7	61.2	1.2	68.9	5.0
V16-1	-404	113	76	49	0.68	7.53	0.01	19.1	0.7	105.1	1.0	573.0	35.0	44	31.4	0.5	46.2	3.4
V16-2	-404	162	105	53	0.70	4.16	0.01	8.2	0.2	50.8	0.9	329.1	15.1	20	37.5	0.5	53.5	3.6
V16-3	-404	376	179	106	0.85	3.21	0.01	6.3	0.1	21.7	0.3	546.1	21.8	11	48.9	0.8	57.5	1.5
V16-4	-404	139	84	48	0.67	12.38	0.02	21.4	0.6	130.8	3.3	566.7	18.2	52	43.3	0.8	64.6	4.4
V16-5	-404	152	79	46	0.66	4.03	0.01	7.1	0.3	37.7	0.8	719.4	20.1	16	43.9	0.6	66.9	2.9
V16-6	-404	146	69	45	0.65	14.95	0.02	22.8	0.5	145.9	1.3	789.4	34.9	57	47.7	0.5	73.7	6.5
V16-7	-404	136	85	49	0.67	6.87	0.01	8.7	0.6	49.2	1.3	477.5	23.6	20	61.2	2.0	90.7	6.7
V17-1	-695	176	95	55	0.72	1.15	0.00	5.0	0.2	17.4	0.3	333.5	9.8	9	22.7	0.6	31.7	2.3
V17-2	-695	191	117	67	0.77	1.72	0.00	6.3	0.2	21.7	0.3	429.5	10.8	11	27.1	0.4	35.4	2.5
V17-3	-695	142	111	72	0.78	1.56	0.01	5.6	0.1	16.3	0.3	306.9	15.1	9	29.6	0.5	37.8	2.7
V17-4	-695	149	105	59	0.73	1.94	0.00	5.9	0.3	27.8	0.9	324.9	12.6	12	28.1	0.8	38.4	2.8
V17-5	-695	106	91	50	0.69	3.32	0.01	11.5	0.4	37.8	0.9	643.7	25.7	20	28.8	0.6	42.0	1.8
V17-6	-695	154	119	66	0.76	2.49	0.01	7.4	0.3	27.7	0.5	329.4	8.2	14	32.4	0.8	42.5	3.2
V17-7	-695	213	124	71	0.78	2.54	0.00	6.7	0.2	19.3	0.3	510.1	15.3	11	39.5	0.7	50.6	1.7
V17-8	-695	338	133	80	0.80	4.39	0.01	8.5	0.2	27.4	0.3	523.7	23.6	15	51.5	0.7	64.2	1.8
V17-9	-695	274	146	85	0.81	3.33	0.01	4.8	0.1	17.9	0.2	225.8	5.0	9	66.5	0.9	81.7	5.9

"Cor. Age" = Ft corrected age assuming no zoning

Supplementary Table DR2: Apatite Fission Track Ages

V13

ζ:	98.4	1σ:	1.7	ρ_d:	3704000
N_s	N_i	Age (Ma)	-95%	95%	Cl (wt%)
6	12	90.5	-57.1	153.0	0
11	30	66.5	-33.7	67.8	0
12	31	70.2	-34.7	68.1	0
7	21	60.5	-35.2	83.8	0
17	56	55.1	-23.5	40.9	0
22	31	128.0	-54.8	95.0	0
13	32	73.6	-35.5	68.3	0
26	48	98.0	-37.9	61.5	0
9	28	58.3	-31.2	66.9	0
14	25	101.3	-49.3	95.4	0
9	23	70.9	-38.6	84.3	0
14	18	140.2	-71.3	144.0	0
8	17	85.2	-49.0	114.0	0
18	43	75.8	-32.7	57.1	0
30	65	83.6	-30.0	46.7	0
Central Age ± 1σ:			**81.5**	**+8 / -6.6 Ma**	

V15

ζ:	98.4	1σ:	1.7	ρ_d:	3811000
N_s	N_i	Age (Ma)	-95%	95%	Cl (wt%)
10	26	71.7	-37.7	78.8	0
14	49	53.4	-24.3	44.5	0
7	22	59.4	-34.5	81.6	0
9	52	32.4	-16.7	34.3	0
8	22	67.8	-38.1	86.5	0
9	27	62.2	-33.4	71.8	0
18	32	104.6	-46.6	83.6	0
11	29	70.7	-35.9	72.6	0
24	50	89.4	-35.1	57.6	0
6	22	50.9	-30.7	76.6	0
6	32	35.1	-20.7	50.2	0
12	35	64.0	-31.3	60.8	0
7	32	40.9	-23.2	53.2	0
23	30	142.2	-60.5	104.0	0
9	17	98.5	-55.3	125.0	0
14	35	74.6	-35.0	65.6	0
12	27	82.8	-41.5	82.5	0
19	69	51.4	-20.9	35.1	0
11	23	89.1	-46.3	95.6	0
7	16	81.5	-48.6	119.0	0
Central Age ± 1σ:			**68.0**	**+6.2 / -5.2 Ma**	

V17

ζ:	98.4	1σ:	1.7	ρ_d:	3891000
N_s	N_i	Age (Ma)	-95%	95%	Cl (wt%)
5	19	50.2	-31.8	86.4	0
7	23	58.0	-33.5	79.1	0
8	18	84.5	-48.4	112.0	0
9	20	85.6	-47.2	104.0	0
6	16	71.4	-44.0	113.0	0
5	14	68.0	-44.0	123.0	0
12	23	99.1	-50.5	102.0	0
7	18	74.0	-43.6	105.0	0
9	29	59.1	-31.6	67.5	0
12	49	46.7	-22.2	42.3	0
11	40	52.4	-25.9	51.1	0
14	24	110.7	-54.2	105.0	0
7	24	55.6	-32.1	75.3	0
21	80	50.1	-19.5	31.9	0
8	14	108.5	-63.7	152.0	0
4	24	31.8	-21.0	61.7	0
5	36	26.5	-16.3	42.3	0
18	40	85.6	-37.1	65.3	0
16	61	50.0	-21.6	37.8	0
9	23	74.5	-40.6	88.4	0
Central Age ± 1σ:			**61.8**	**+6.1 / -5.1 Ma**	

Supplementary Table DR3: U-Pb zircon data collected by LA-ICPMS

VT11-13

Isotope Ratios							Apparent Ages									Concentrations	
$^{207}Pb/^{235}U$	2σ	$^{206}Pb/^{238}U$	2σ	Correl.	$^{207}Pb/^{206}Pb$	2σ	$^{207}Pb/^{235}U$ (Ma)	2σ (Ma)	$^{206}Pb/^{238}U$ (Ma)	2σ (Ma)	$^{207}Pb/^{206}Pb$ (Ma)	2σ (Ma)	$^{207}Corr$ (Ma)	2σ (Ma)	conc. (%)	U (ppm)	Th (ppm)
0.5300	0.0570	0.0310	0.0004	0.05	0.1230	0.0140	417	37	196.7	2.5	1780	220	428.9	43.7	52.8	671	614
0.2423	0.0075	0.0309	0.0003	0.70	0.0566	0.0016	219.9	6.1	196.4	2	452	61	219.6	6.3	10.7	602	190
0.2530	0.0130	0.0292	0.0005	-0.11	0.0615	0.0033	228	11	185.7	3.3	607	98	224.8	11.9	18.6	636	252
0.2131	**0.0051**	**0.0299**	**0.0004**	**0.54**	**0.0513**	**0.0010**	**196**	**4.3**	**190.1**	**2.7**	**246**	**45**	**194.9**	4.3	**3.0**	**510**	**180**
0.2285	**0.0043**	**0.0295**	**0.0004**	**0.61**	**0.0559**	**0.0008**	**208.8**	**3.5**	**187.1**	**2.3**	**440**	**33**	**207.6**	**4.1**	**10.4**	**566**	**194**
0.5700	0.0210	0.0335	0.0005	0.49	0.1200	0.0040	456	13	212.5	2.9	1946	59	448.0	21.7	53.4	340	168
0.2048	0.0061	0.0264	0.0003	0.25	0.0541	0.0015	188.9	5.1	168.1	2.1	369	62	182.6	5.3	11.0	262	147
0.3660	0.0150	0.0350	0.0006	0.56	0.0744	0.0026	318	12	222	3.6	1063	65	311.8	12.8	30.2	194	308
0.2236	0.0075	0.0292	0.0004	0.36	0.0539	0.0016	204.5	6.2	185.4	2.7	344	66	199.2	6.1	9.3	245	185
0.2140	**0.0038**	**0.0299**	**0.0005**	**0.55**	**0.0507**	**0.0009**	**197.3**	**3.3**	**189.9**	**3.1**	**214**	**41**	**192.6**	4.3	**3.8**	**973**	**471**
									Weighted Mean (n=3):				**198.4**	**4.7**			

VT11-14

Isotope Ratios							Apparent Ages									Concentrations	
$^{207}Pb/^{235}U$	2σ	$^{206}Pb/^{238}U$	2σ	Correl.	$^{207}Pb/^{206}Pb$	2σ	$^{207}Pb/^{235}U$ (Ma)	2σ (Ma)	$^{206}Pb/^{238}U$ (Ma)	2σ (Ma)	$^{207}Pb/^{206}Pb$ (Ma)	2σ (Ma)	$^{207}Corr$ (Ma)	2σ (Ma)	conc. (%)	U (ppm)	Th (ppm)
0.2031	**0.0065**	**0.0285**	**0.0004**	**0.25**	**0.0504**	**0.0016**	**187.5**	**5.5**	**181.2**	**2.4**	**213**	**63**	**181.1**	**2.4**	**3.4**	**199**	**111**
0.2035	**0.0054**	**0.0298**	**0.0004**	**0.22**	**0.0488**	**0.0014**	**187.8**	**4.6**	**189.4**	**2.6**	**136**	**60**	**189.7**	**2.7**	**0.9**	**271**	**138**
0.2277	0.0086	0.0298	0.0005	0.28	0.0553	0.0022	209	6.8	189.4	2.9	390	81	188.1	2.9	9.4	120	61
0.2810	0.0110	0.0313	0.0005	0.20	0.0651	0.0024	250.6	8.4	198.5	3.1	787	77	194.9	3.1	20.8	146	64
0.2065	0.0090	0.0283	0.0004	0.28	0.0524	0.0021	191	7.4	179.9	2.7	289	87	179.4	2.7	5.8	112	49
0.3440	0.0120	0.0315	0.0005	0.28	0.0772	0.0026	299.6	9.1	200.1	3.3	1123	64	193.4	3.3	33.2	100	54
0.2165	0.0077	0.0286	0.0005	0.06	0.0548	0.0022	199.6	6.6	181.8	3.2	383	86	180.7	3.2	8.9	120	52
0.3580	0.0180	0.0310	0.0007	0.60	0.0837	0.0039	309	13	196.4	4.1	1257	93	188.3	4.1	36.4	69	35
0.2082	**0.0066**	**0.0291**	**0.0004**	**0.30**	**0.0518**	**0.0017**	**191.8**	**5.6**	**184.6**	**2.8**	**266**	**70**	**184.2**	**2.8**	**3.8**	**180**	**100**
0.2030	**0.0075**	**0.0295**	**0.0004**	**0.26**	**0.0494**	**0.0018**	**187.2**	**6.3**	**187.5**	**2.6**	**169**	**74**	**187.3**	**2.6**	**0.2**	**165**	**83**
									Weighted Mean: (n=4)				**185.6**	**1.9**			

VT11-15

Isotope Ratios							Apparent Ages									Concentrations	
$^{207}Pb/^{235}U$	2σ	$^{206}Pb/^{238}U$	2σ	Correl.	$^{207}Pb/^{206}Pb$	2σ	$^{207}Pb/^{235}U$ (Ma)	2σ (Ma)	$^{206}Pb/^{238}U$ (Ma)	2σ (Ma)	$^{207}Pb/^{206}Pb$ (Ma)	2σ (Ma)	$^{207}Corr$ (Ma)	2σ (Ma)	conc. (%)	U (ppm)	Th (ppm)
0.1928	**0.0091**	**0.0275**	**0.0004**	**0.19**	**0.0499**	**0.0023**	**178.4**	**7.7**	**174.8**	**2.3**	**175**	**93**	**175.8**	**7.8**	**2.0**	**125**	**63**
0.2090	0.0160	0.0280	0.0005	0.17	0.0533	0.0039	195	13	178.1	3	360	140	190.1	13.1	8.7	85	62
0.1620	0.0200	0.0275	0.0009	-0.15	0.0433	0.0058	150	17	174.6	5.7	-90	210	154.2	19.8	16.4	27	36
0.2140	0.0210	0.0286	0.0006	0.21	0.0547	0.0054	197	17	181.9	3.7	350	170	198.5	18.2	7.7	55	74
0.2066	**0.0039**	**0.0287**	**0.0004**	**0.37**	**0.0530**	**0.0010**	**190.6**	**3.3**	**182.6**	**2.3**	**318**	**41**	**193.4**	**4.0**	**4.2**	**1261**	**810**
0.2140	0.0280	0.0284	0.0009	0.47	0.0565	0.0072	192	23	180.5	5.9	420	220	202.9	24.3	6.0	56	33
0.2290	0.0180	0.0288	0.0005	0.35	0.0591	0.0044	205	14	182.8	2.9	470	140	213.9	15.0	10.8	190	63
0.2040	**0.0230**	**0.0297**	**0.0008**	**0.09**	**0.0513**	**0.0059**	**187**	**20**	**188.9**	**4.9**	**230**	**220**	**193.9**	**20.8**	**1.0**	**70**	**40**
0.2100	**0.0380**	**0.0282**	**0.0009**	**0.30**	**0.0580**	**0.0110**	**185**	**30**	**179.5**	**5.9**	**380**	**320**	**206.8**	**36.1**	**3.0**	**48**	**40**
0.2049	**0.0091**	**0.02897**	**0.00045**	**0.1878**	**0.0516**	**0.0023**	**190.7**	**7.7**	**184.1**	**2.8**	**243**	**93**	**190.3**	**8.2**	**3.5**	**927**	**456**
									Weighted Mean (n=5):				**192.0**	**4.9**			

VT11-16

Isotope Ratios							Apparent Ages									Concentrations	
$^{207}Pb/^{235}U$	2σ	$^{206}Pb/^{238}U$	2σ	Correl.	$^{207}Pb/^{206}Pb$	2σ	$^{207}Pb/^{235}U$ (Ma)	2σ (Ma)	$^{206}Pb/^{238}U$ (Ma)	2σ (Ma)	$^{207}Pb/^{206}Pb$ (Ma)	2σ (Ma)	$^{207}Corr$ (Ma)	2σ (Ma)	conc. (%)	U (ppm)	Th (ppm)
0.2016	**0.0056**	**0.0290**	**0.0004**	**0.36**	**0.0506**	**0.0013**	**186.9**	**4.8**	**184.5**	**2.4**	**211**	**56**	**187.3**	**4.9**	**1.3**	**725**	**361**
0.2134	0.0059	0.0289	0.0004	0.28	0.0526	0.0014	196.2	4.9	183.9	2.8	297	57	193.5	5.5	6.3	798	489
0.2480	0.0140	0.0286	0.0005	0.53	0.0612	0.0030	226	12	181.6	2.8	600	100	219.4	10.7	19.6	587	301
0.2079	**0.0054**	**0.0292**	**0.0005**	**0.48**	**0.0493**	**0.0011**	**191.5**	**4.5**	**185.5**	**3.2**	**158**	**48**	**183.8**	**4.8**	**3.1**	**1248**	**765**
0.2126	0.0062	0.0291	0.0004	0.22	0.0506	0.0016	195.5	5.2	185.1	2.8	210	65	187.9	6.0	5.3	743	248
0.2090	**0.0058**	**0.0291**	**0.0005**	**0.32**	**0.0496**	**0.0013**	**192.5**	**4.9**	**184.9**	**2.8**	**173**	**55**	**184.3**	**5.1**	**3.9**	**898**	**417**
0.2181	0.0064	0.0293	0.0005	0.53	0.0522	0.0013	200.1	5.3	186.4	3.1	280	55	194.5	5.4	6.8	962	485
0.2062	**0.0060**	**0.0300**	**0.0004**	**0.17**	**0.0496**	**0.0014**	**190.1**	**5.1**	**190.6**	**2.7**	**169**	**64**	**189.5**	**5.5**	**0.3**	**889**	**513**
0.2019	**0.0064**	**0.0300**	**0.0005**	**0.48**	**0.0494**	**0.0014**	**186.4**	**5.4**	**190.8**	**3.2**	**161**	**60**	**189.0**	**5.7**	**2.4**	**1733**	**886**
0.1996	**0.0062**	**0.0293**	**0.0004**	**0.26**	**0.0513**	**0.0016**	**184.5**	**5.3**	**185.9**	**2.6**	**242**	**69**	**191.0**	**6.0**	**0.8**	**3036**	**1265**
									Weighted Mean (n=6):				**187.5**	**1.2**			

VT11-17

Isotope Ratios							Apparent Ages									Concentrations	
$^{207}Pb/^{235}U$	2σ	$^{206}Pb/^{238}U$	2σ	Correl.	$^{207}Pb/^{206}Pb$	2σ	$^{207}Pb/^{235}U$ (Ma)	2σ (Ma)	$^{206}Pb/^{238}U$ (Ma)	2σ (Ma)	$^{207}Pb/^{206}Pb$ (Ma)	2σ (Ma)	$^{207}Corr$ (Ma)	2σ (Ma)	conc. (%)	U (ppm)	Th (ppm)
0.2140	**0.0130**	**0.0313**	**0.0006**	**-0.10**	**0.0540**	**0.0037**	**199**	**11**	**198.9**	**3.7**	**340**	**140**	**212.9**	**13.7**	**0.1**	**2439**	**-6800**
0.2030	**0.0100**	**0.0303**	**0.0004**	**-0.05**	**0.0527**	**0.0027**	**186.8**	**8.4**	**192.1**	**2.4**	**330**	**110**	**201.7**	**9.7**	**2.8**	**-8760**	**-1730**
0.6670	0.0640	0.0354	0.0012	0.38	0.1530	0.0140	510	40	224.3	7.8	2330	170	566.4	48.0	56.0	-279	-117
0.5050	0.0240	0.0344	0.0006	0.18	0.1185	0.0058	419	17	217.7	4	1929	83	452.3	25.7	48.0	-696	-291
0.1970	**0.0170**	**0.0303**	**0.0007**	**0.09**	**0.0519**	**0.0047**	**184**	**14**	**192.1**	**4.5**	**320**	**180**	**199.0**	**16.9**	**4.4**	**-474**	**-229**
0.1996	**0.0088**	**0.0284**	**0.0004**	**0.12**	**0.0496**	**0.0023**	**184.3**	**7.4**	**180.6**	**2.4**	**170**	**91**	**180.3**	**8.0**	**2.0**	**101**	**64**
0.2087	0.0095	0.0279	0.0005	0.15	0.0532	0.0025	192.9	7.8	177.2	3.2	313	95	188.9	8.7	8.1	128	48
0.2100	0.0093	0.0264	0.0005	-0.27	0.0560	0.0030	193.3	7.8	167.9	3.2	440	110	188.2	10.0	13.1	219	131
0.2150	**0.0110**	**0.0302**	**0.0006**	**0.20**	**0.0520**	**0.0026**	**197.3**	**9.1**	**191.5**	**3.9**	**250**	**100**	**198.7**	**9.8**	**2.9**	**118**	**107**
0.3290	0.0130	0.0291	0.0003	0.15	0.0806	0.0031	288	10	185.1	2.1	1195	76	284.8	13.1	35.7	250	267
									Weighted Mean (n=5):				**198.5**	**5.2**			

"Correl" = Error Correlation between 207/235 and 206/238 ratios

"conc." = denotes % concordance between 207/235 and 206/238 ages

"207Corr" = denotes the 206/238 age after correction for an assumed intial 207/206 raio of 0.847 using the Age7corr function in Isoplot